Supporting Information

Dual Atom Cu-Fe Ensemble Sites for Enhanced Efficiency of Green Ammonia Production from Tandem Electrochemical Nitrate Reduction Process

Junbeom Maeng[+], Jaehyun Heo[+], Minguk Kwak[+], Jungseub Ha, Taehun Kim, Junhyuk Ji, Hansol Bae, Jeongbin Cho and Won Bae Kim*

J. Maeng, J. Heo, J. Ha, J. Ji, H. Bae, J. Cho and Prof. W. B. Kim*
Department of Chemical Engineering, Pohang University of Science and Technology (POSTECH), 77 Cheongam-ro, Nam-gu, Pohang-si, Gyeongsangbuk-do 37673, Republic of Korea

M. Kwak, T. Kim and Prof. W. B. Kim*
Graduate Institute of Ferrous & Eco Materials Technology, Pohang University of Science and Technology (POSTECH), 77 Cheongam-ro, Nam-gu, Pohang-si, Gyeongsangbuk-do 37673, Republic of Korea

E-mail: kimwb@postech.ac.kr (W. B. Kim)
[+] These authors contributed equally to this work.

Keywords
Green ammonia, Nitrate reduction, Dual atom catalyst, Tandem reaction, Synergistic effect.

1. Experimental section

1.1. Chemicals and materials

Potassium nitrite (KNO_2, Sigma Aldrich), potassium nitrate (KNO_3, Sigma Aldrich), potassium hydroxide (KOH, Sigma Aldrich), carbon paper (AvCarb P50T, NARA Cell-Tech Corp.), Iron(III) nitrate nonahydrate ($Fe(NO_3)_3$ $9H_2O$, Sigma Aldrich), Copper(II) nitrate trihydrate ($Cu(NO_3)_2$ $3H_2O$, Sigma Aldrich), D-(+) Glucose ($C_6H_{12}O_6$, JUNSEI), Melamine ($C_3H_6N_6$, Sigma Aldrich), sodium hypochlorite aqueous solution (NaClO 6~14%, Sigma Aldrich), sodium nitroferricyanide ($Na[Fe(NO)(CN)_5]$, Sigma Aldrich), Sodium citrate dihydrate ($C_6H_9Na_3O_9$, Sigma Aldrich), N-(1-naphthyl) ethyldiamine dihydrochloride ($C_{12}H_{14}N_2$, Sigma Aldrich), sulfonamide (Sigma Aldrich), orthophosphoric acid (H_3PO_4, Sigma Aldrich), hydrochloric acid (HCl, Sigma Aldrich) and Nafion 212 membrane (Fuel Cell store) were purchased from the specified suppliers. Deionized water (DI water, 18 MΩ cm, Millipore) was used for entire experimental steps.

1.2 Synthesis of Activated Carbon (AC)

About 15 g of Vulcan X72R carbon was added to a round bottom flask with a heating mantle equipped with a reflux condenser, 300 mL of a solution obtained by diluting distilled water and 65% HNO_3 1:1 was added. The prepared mixture was stirred at 60°C for 6 hours. And washing was performed using a large amount of water, and a freeze dryer was used for 3 days, and the name of the obtained black powder was AC.

1.3 Synthesis of Cu-Fe DAC

In total, 180 mg of AC, 0.45 mmol copper (II) nitrate trihydrate, 0.45 mmol Iron (III) nitrate hexahydrate, and 18 mmol of α-D-glucose were dispersed in 15 mL of distilled water and sonicated for 45 min to get a homogenous black suspension. After several washes with water using a centrifuge, the slurry was harvested and dried overnight in a vacuum oven at 60°C. The black powder and melamine were mixed at a mass ratio of 1:5. The mixed powder was placed in a tube furnace and stayed at 800℃ at Ar atmosphere with ramping rate 5℃/min, naturally cooled down to the room temperature. The obtained black powder was named Cu-Fe DAC. The Cu SAC was using 0.9 mmol copper (II) nitrate trihydrate, Fe SAC was using Iron (III) nitrate hexahydrate, and the rest of procedure were same.

1.4 Catalyst characterizations

Scanning electron microscopy (SEM) images were collected using HITACHI S-4800 instrument operated at 5 kV. High-resolution transmission electron microscopy (HR-TEM) with element mapping analysis was performed using JEM-2200FS instrument operated at 200 kV. X-ray diffraction (XRD) data were collected on a Bruker-Advanced D8 diffractometer using a Cu Kα (λ = 1.5418 Å) radiation operated at 40 kV and 100 mA. High-performance X-ray photoelectron spectrometer (HP-XPS, K-ALPHA+) was used in order to obtain the XPS spectra of the surface elements. The synchrotron EXAFS and XANES spectra of Cu K-edge and Fe K-edge were obtained on the 7D, 8C, 10C beamline of the Pohang Accelerator Laboratory (PLS-II), Republic of Korea.

1.5 Electrochemical measurements

The electrochemical measurements were performed in three electrodes H-type cell which was separated by Nafion 212 membrane into two compartments. Cu-Fe DAC, Cu SAC and Fe SAC catalysts deposited on carbon paper (geometric area = 1 cm x 1 cm) were used as the working electrode. Pt coil and Hg/HgO (1 M NaOH) electrode were used as the counter and reference electrodes, respectively. The potential was converted to RHE by the following equation:

$$E\ (\text{vs RHE}) = E\ (\text{vs Hg/HgO}) + 0.140\ \text{V} + 0.0591 \times \text{pH}$$

A ZIVELAB potentiostat was used to record the electrochemical response. Linear sweep voltammetry (LSV) was carried out from 0 V to -1.6 V vs Hg/HgO at a scan rate of 20 mV s^{-1}. For electrocatalytic nitrate reduction, 10 mL of 1 M KOH aqueous solution was filled in the anode compartment, and 10 mL of 1 M KOH aqueous solution containing 0.1 M KNO_3 was filled in the cathode compartment. The chronoamperometry tests were conducted at constant potentials for 1 h at room temperature. For stability test, the chronoamperometry was performed 6 times at -0.53 V vs RHE for 1 h each. The products obtained from the electrochemical NO_3^- reduction were detected and analyzed by UV-visible spectroscopy (Agilent Technologies Cary 8454) using indophenol blue method and Griess method.

1.6 Ammonia (NH_3) detection by Indophenol blue method

0.05 mL of electrolyte was diluted to 10 mL (200 times) using 1 M KOH solution for the detection. Then, 2 mL of 1 M NaOH solution containing 5 wt% salicylic acid and 5 wt% sodium citrate was prepared, followed by addition of 1 mL of 0.05 M NaClO and 0.01 mL of 1 wt% sodium nitroferricyanide aqueous solution. After 2 hours at room temperature, the absorbance of solution was detected by UV–visible spectroscopy (Agilent Technologies Cary 8454). The absorbance at a wavelength of 655 nm was used to calculate the ammonia concentration. The calibration curve was obtained by using the ammonium chloride aqueous solutions of known concentration.

1.7 Nitrite (NO_2^-) detection by Griess method

The Griess color reagent was prepared by N-(1-naphthyl) ethylenediamine dihydrochloride (0.04 g), sulfonamide (0.8 g), and H_3PO_4 (85%, 2 mL) into DI water (10 mL). Before the test, 100 μL of electrolytes were mixed with 100 μL of HCl. The neutral solutions were diluted to 2 mL and then mixed with the 40 μL of Griess agent. After 10 minutes at room temperature, the absorbance of solution was detected by UV–visible spectroscopy (Agilent Technologies Cary 8454). The absorbance at a wavelength of 540 nm was used to calculate the nitrite concentration. The calibration curve was obtained by using the potassium nitrite aqueous solutions of known concentration.

1.8 Calculation of the NH_3 faradaic efficiency and yield

The NH_3 faradaic efficiency was calculated as follows:

$$NH_3\ Faradaic\ efficiency = (n \times F \times C_{NH_3} \times V)/Q \times 100\%$$

The yield of NH_3 was calculated as follows:

$$NH_3\ yield\ (\mu g\ cm^{-1}\ h^{-1}) = \left(C_{NH_3} \times V \times M_{NH_3}\right)/(t \times A)$$

C_{NH_3} is the concentration of NH_3 (μg/mL), n is 8 which is the number of electrons transferred to generate 1 mol NH_3, F is the Faradaic constant (96485 C/mol), V is the volume of electrolyte, Q is the total electric charge passing through the electrode, M_{NH_3} is the molar mass of NH_3, t is the reaction time, A is the surface area of catalyst.

1.9 Calculation of the NO_2^- faradaic efficiency

The NH_3 faradaic efficiency was calculated as follows:

$$NO_2^- \; Faradaic\; efficiency = (n \times F \times C_{NO_2^-} \times V)/Q \times 100\%$$

$C_{NO_2^-}$ is the concentration of NO_2^- (μg/mL), n is 2 which is the number of electrons transferred to generate 1 mol NO_2^-, F is the Faradaic constant (96485 C/mol), V is the volume of electrolyte, Q is the total electric charge passing through the electrode.

1.10 Computational Methods

Activated carbon-supported single-atom catalysts (SACs) containing Fe or Cu coordinated by four nitrogen atoms, as well as a dual-atom catalyst (DAC) containing Cu–Fe coordinated by six nitrogen atoms, were constructed to model the active sites for nitrate reduction reaction (NO_3RR). Spin-polarized plane-wave density-functional-theory (DFT) calculations were carried out with the Quantum ESPRESSO suite[1]. The ion-electron interactions were treated using projector augmented wave (PAW) method[2]. Exchange–correlation energies were evaluated within the generalized-gradient-approximation (GGA) using the functional Perdew–Burke–Ernzerhof (PBE), and the van der Waals interaction was included using the Grimme-D3 dispersion correction[3-5]. Pseudopotentials were selected from the Standard Solid-State Pseudopotential (SSSP) library[6].

A kinetic energy cutoff of 520 eV for the plane-wave expansion was set, and The Brillouin zones were sampled by the Monkhorst−Pack k-points mesh of 3×3×1[7]. The convergence criteria were set to 1×10^{-5} eV atom^{-1}, 3×10^{-2} eV Å^{-1} for the total energy and forces, respectively. A vacuum spacing of at least 15 Å was applied along the z-axis to eliminate interactions between periodic images of the slab.

The adsorption energy E_{ads} was calculated by using the following formula:

$$E_{ads} = E_{slab\text{-}molecule} - E_{slab} - E_{molecule}$$

Where $E_{slab\text{-}molecule}$ represents the total energy of adsorbed system. E_{slab} represents the calculated energies of Cu-SAC/NC, Fe-SAC/NC and Cu-Fe DAC/NC. $E_{molecule}$ represents the calculated energy of NO_3 molecule. A more negative value of E_{ads} represents stronger adsorption.

Based on computational hydrogen electrode (CHE) model[8], the Gibbs free energy change (ΔG) of each elementary step is defined as

$$\Delta G = \Delta E_{DFT} + \Delta ZPE - T\Delta S$$

where ΔE_{DFT}, ZPE, T and S are energy obtained from DFT calculations, zero-point energy, temperature (298.15 K), and entropy, respectively.

Here, the element steps of nitrate reduction on oreoared catalysts can be summarized by the following reaction equations.

$$* + NO_3^- \rightarrow *NO_3 + e^-$$

$$*NO_3 + 2H^+ + 2e^- \rightarrow *NO_2 + H_2O$$

$$*NO_2 + 2H^+ + 2e^- \rightarrow *NO + H_2O$$

$$*NO + H^+ + e^- \rightarrow *HNO$$

$$*HNO + H^+ + e^- \rightarrow *H_2NO$$

$$*H_2NO + H^+ + e^- \rightarrow *H_2NOH$$

$$*H_2NOH + H^+ + e^- \rightarrow *NH_2 + H_2O$$

$$*NH_2 + H^+ + e^- \rightarrow *NH_3$$

$$*NH_3 \rightarrow *+ NH_3$$

To avoid calculating the energy of charged NO_3^- directly, gaseous HNO_3 is chosen as a reference based on the following steps[9].

$$HNO_3 \rightarrow H^+ + NO_3^-$$

$$* + NO_3^- \rightarrow *NO_3 + e^-$$

$$* + HNO_3 \rightarrow *NO_3 + H^+ + e^-$$

As a result, the adsorption energy of NO_3^- (ΔG_{*NO3}) can be approximated by

$$\Delta G_{*NO3} = G_{*NO3} - G_* - G_{HNO3} + 0.5G_{H2}$$

where G_{*NO3}, G_*, G_{HNO3}, and G_{H2} are the Gibbs free energy of NO_3^- adsorbed on SAC or DAC, SAC or DAC substrates, HNO_3 and H_2 molecules in the gas phase, respectively.

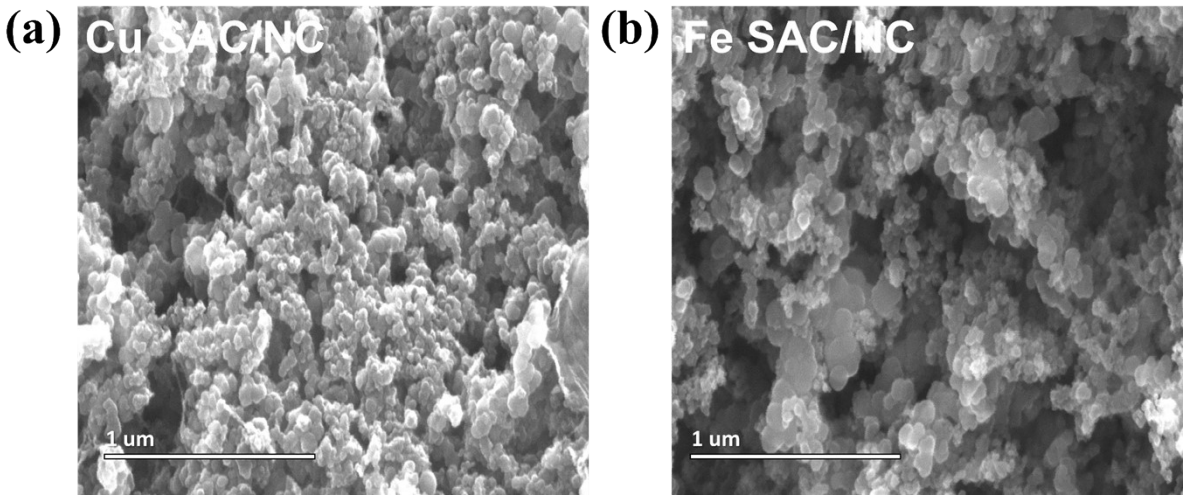

Figure S1. SEM image of (a) Cu SAC/NC. (b) Fe SAC/NC

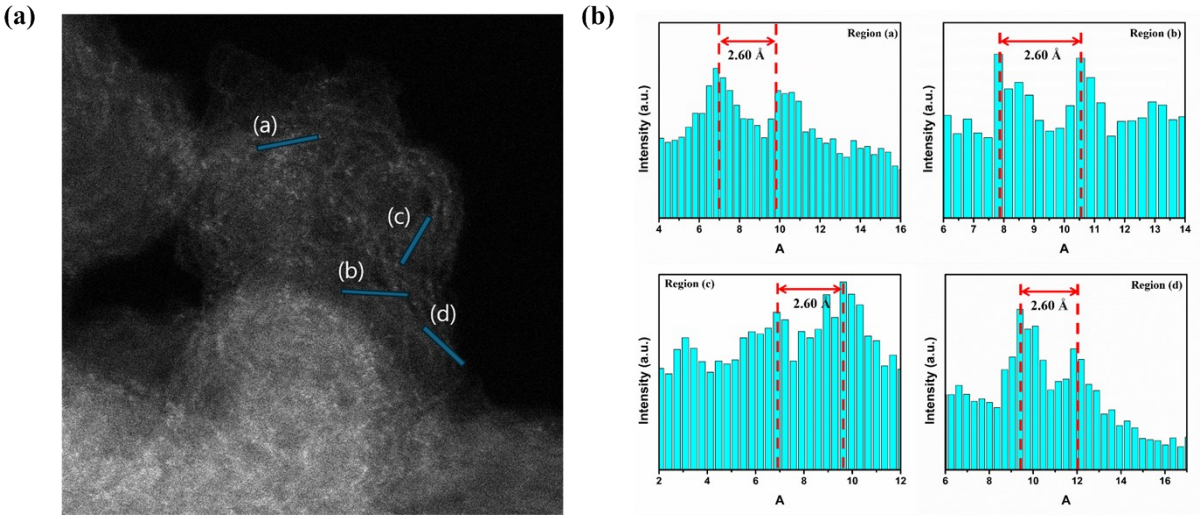

Figure S2. (a) HAADF-STEM image of Cu–Fe DAC/NC (same as Figure 1(c)), (b) Line-scanning based atomic intensity profiles obtained from various regions.

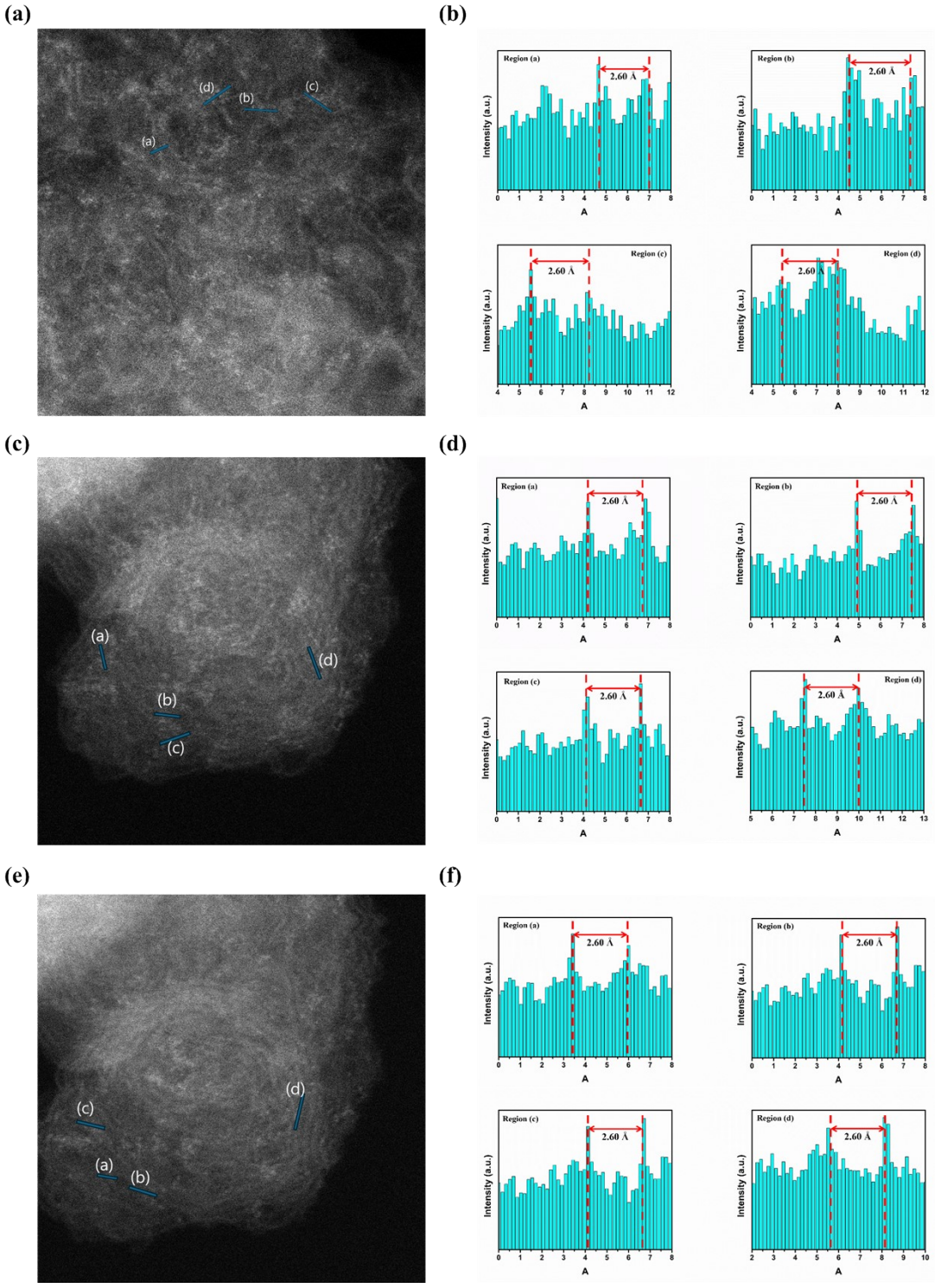

Figure S3. (a), (c), (e) Other HAADF-STEM images of Cu–Fe DAC/NC. (b), (d), (f) Line-scanning based atomic intensity profiles obtained from various regions of each HAADF-STEM images.

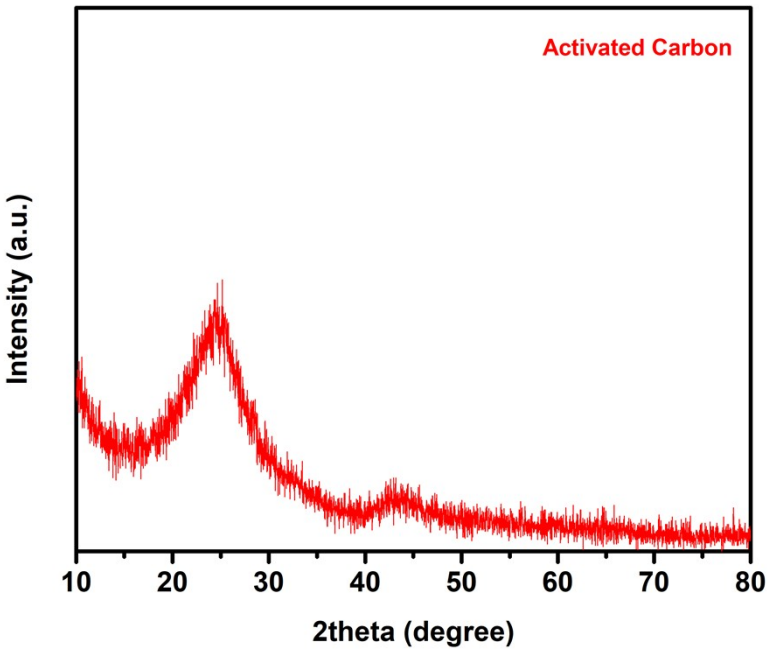

Figure S4. XRD spectra of Activated Carbon

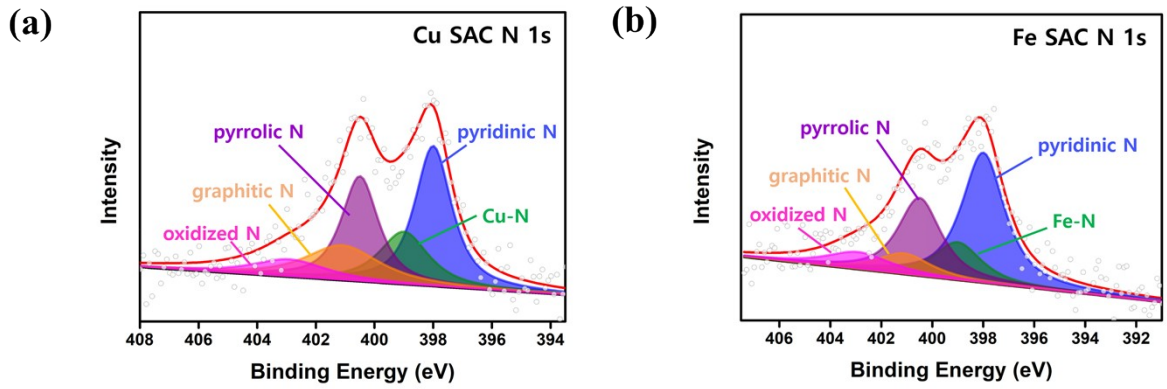

Figure S5. XPS spectra of N 1s (a) Cu SAC/NC (b) Fe SAC/NC

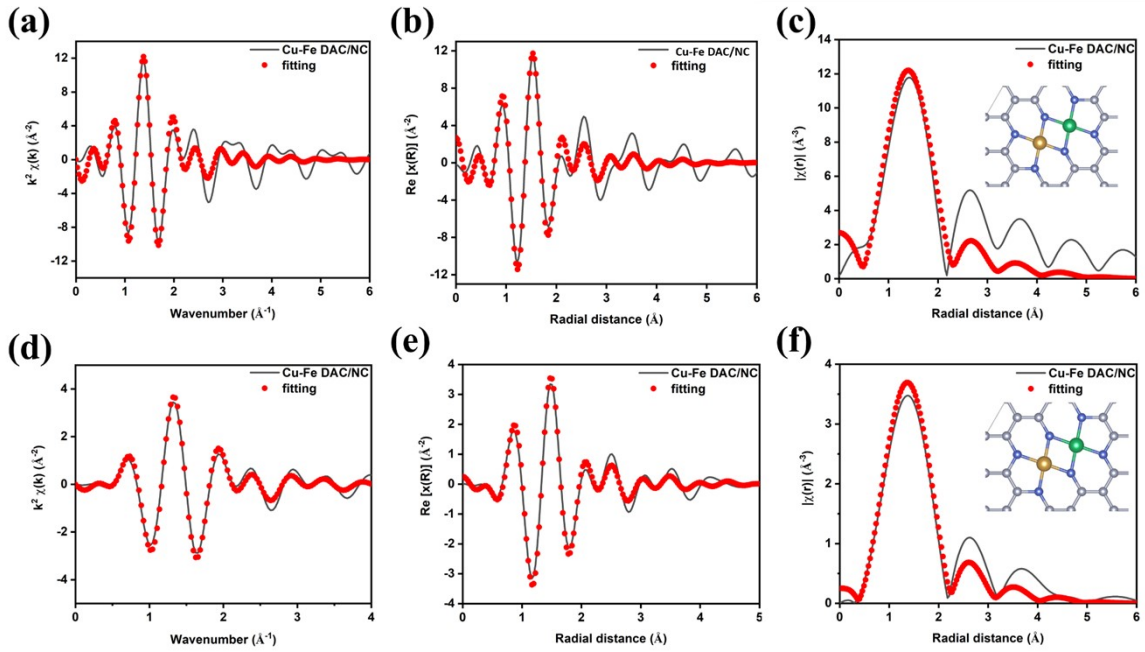

Figure S6. EXAFS fitting curves for the Cu-Fe DAC/NC of (a) *k-space* (b) *R-space* real part (c) *R-space* (inset: proposed model) of Cu K-edge. (d) *k-space* (e) *R-space* real part (f) *R-space* (inset: proposed model) of Fe K-edge.

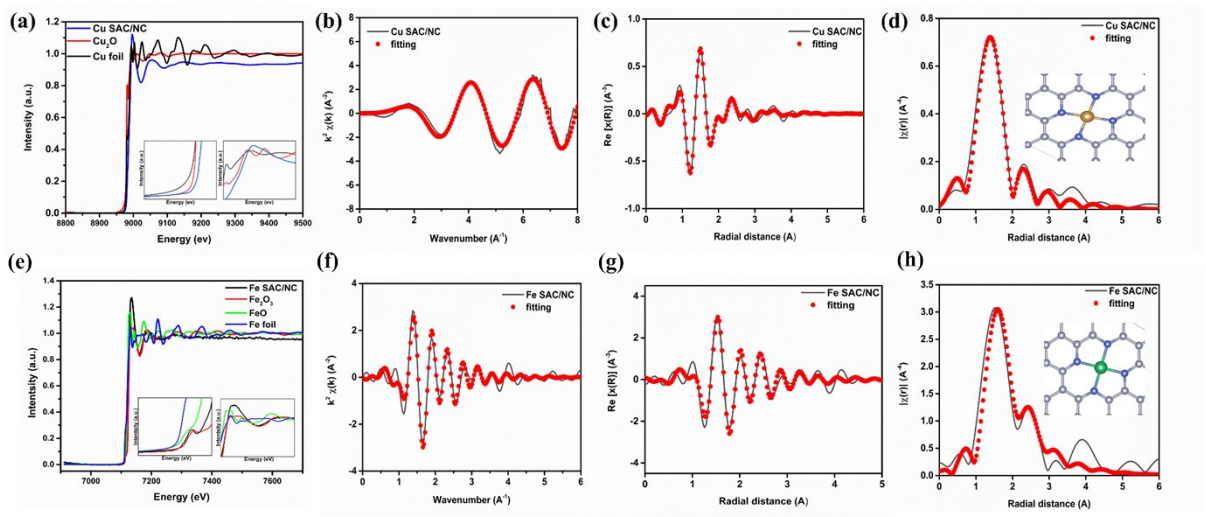

Figure S7. (a) XANES spectra, EXAFS fitting curve of (b) *k-space* (c) *R-space* real part (d) *R-space* (inset: proposed model) of Cu SAC/NC. (e) XANES spectra, EXAFS fitting curve of (f) *k-space* (g) *R-space* real part (h) *R-space* (inset: proposed model) of Fe SAC/NC

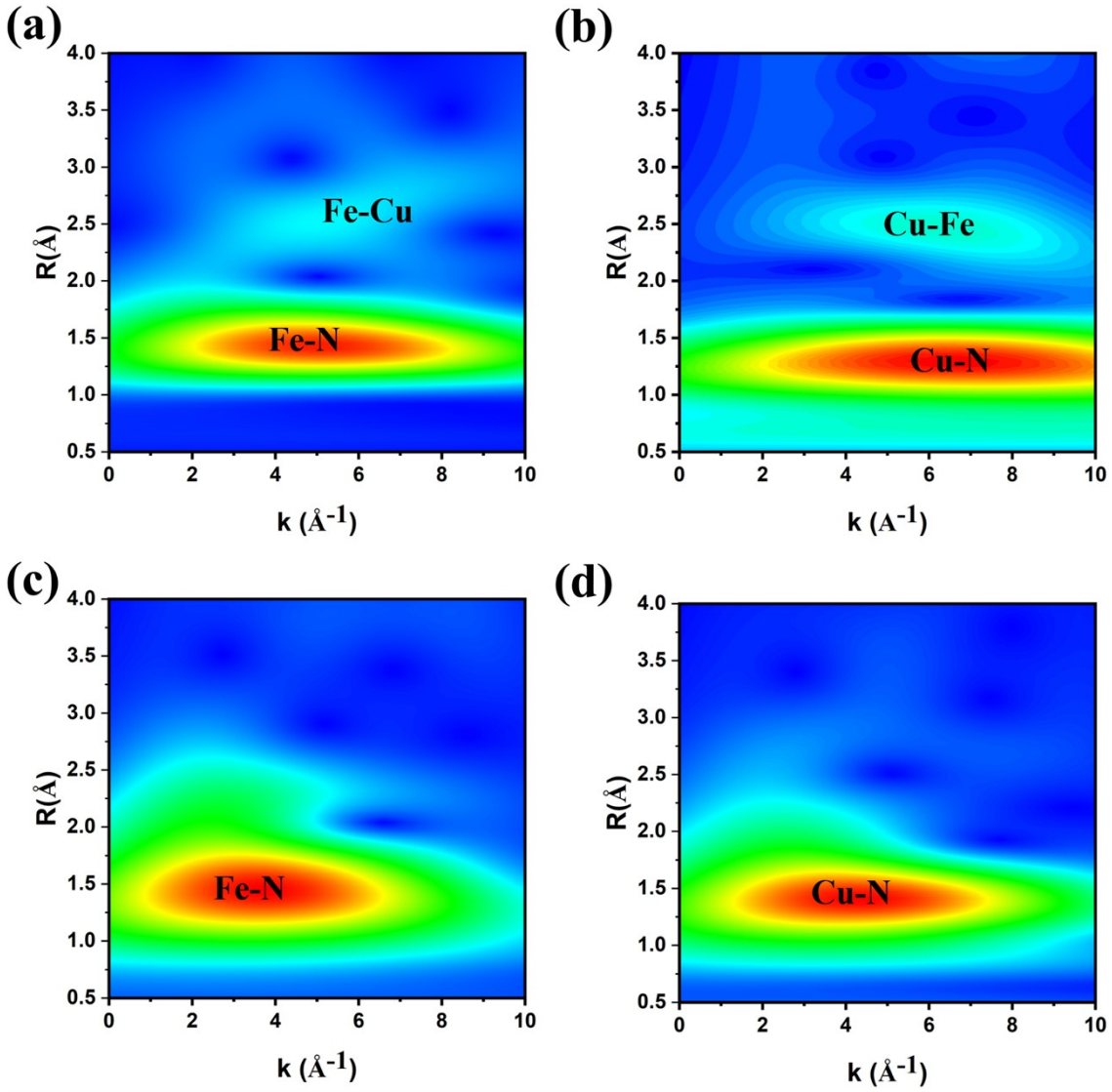

Figure S8. Wavelet transform of the k^2-weighted EXAFS data of (a) Fe K-edge, (b) Cu K-edge of Cu-Fe DAC/NC (c) Fe K-edge of Fe SAC (d) Cu K-edge of Cu SAC

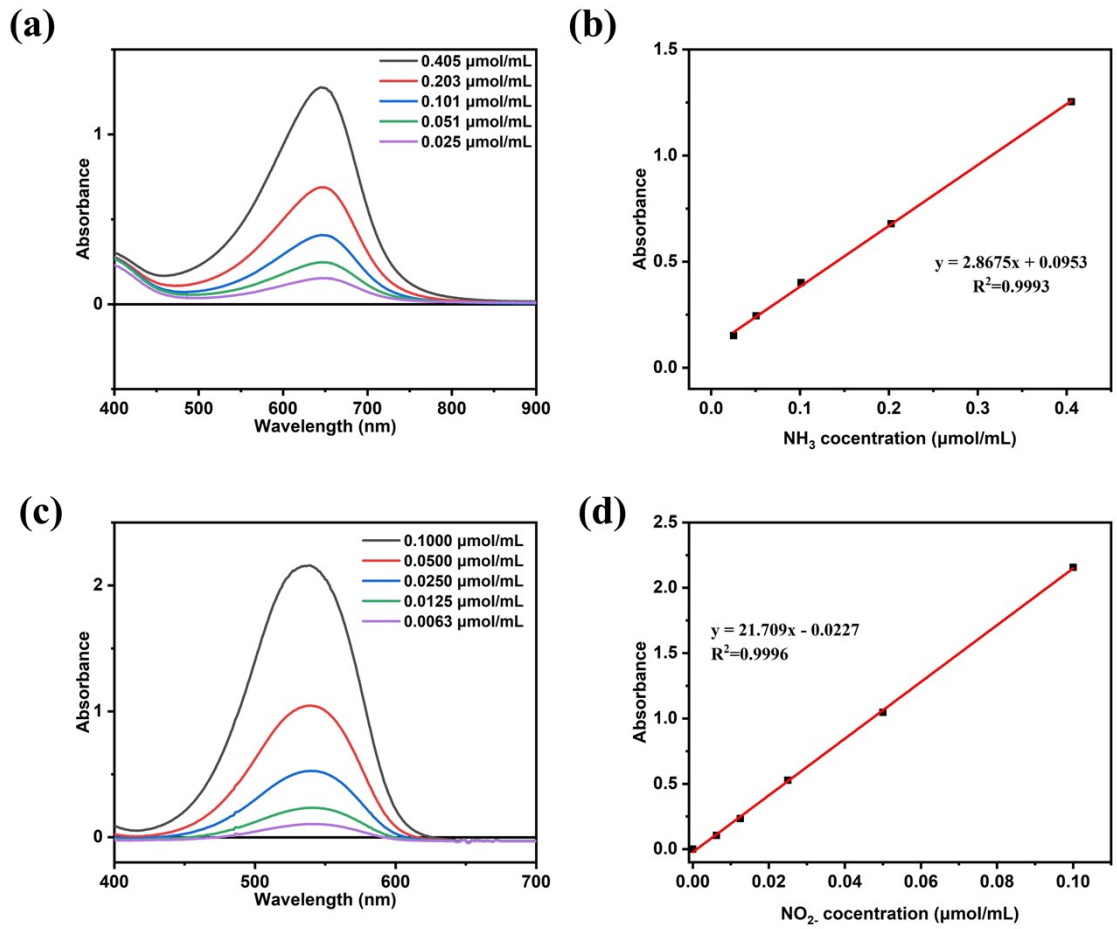

Figure S9. (a) UV-vis absorption spectra and (b) calibration curve of indophenol blue method (c) UV-vis absorption spectra and (d) calibration curve of indophenol Griess method.

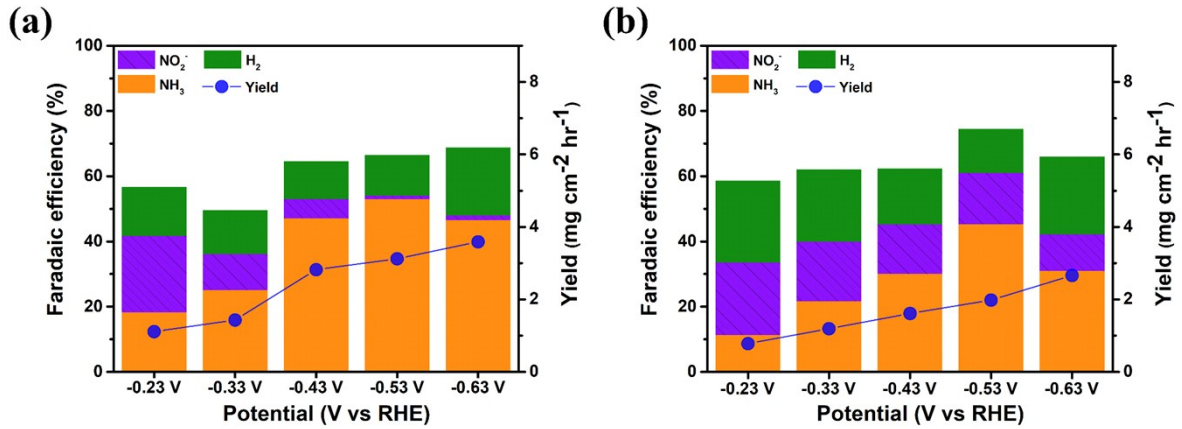

Figure S10. Faradaic efficiency and NH_3 production rate versus applied potential of (a) Fe SAC/NC (b) Cu SAC/NC

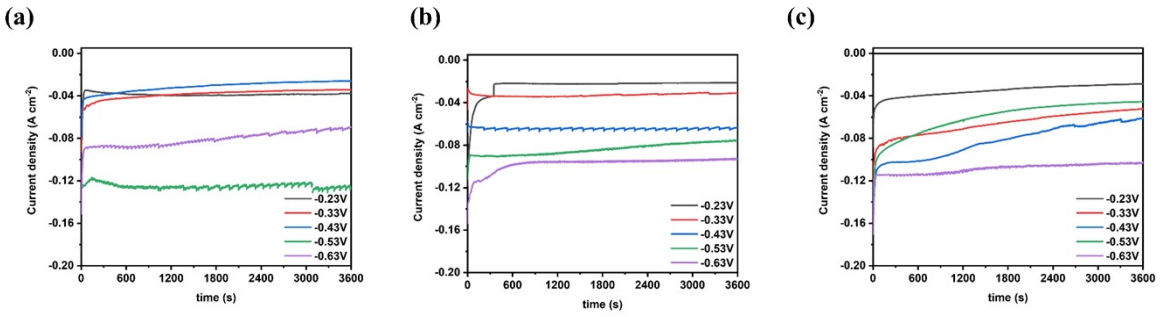

Figure S11. Current densities versus applied potential (a) Cu-Fe DAC/NC (b) Fe SAC/NC (c) Cu SAC/NC

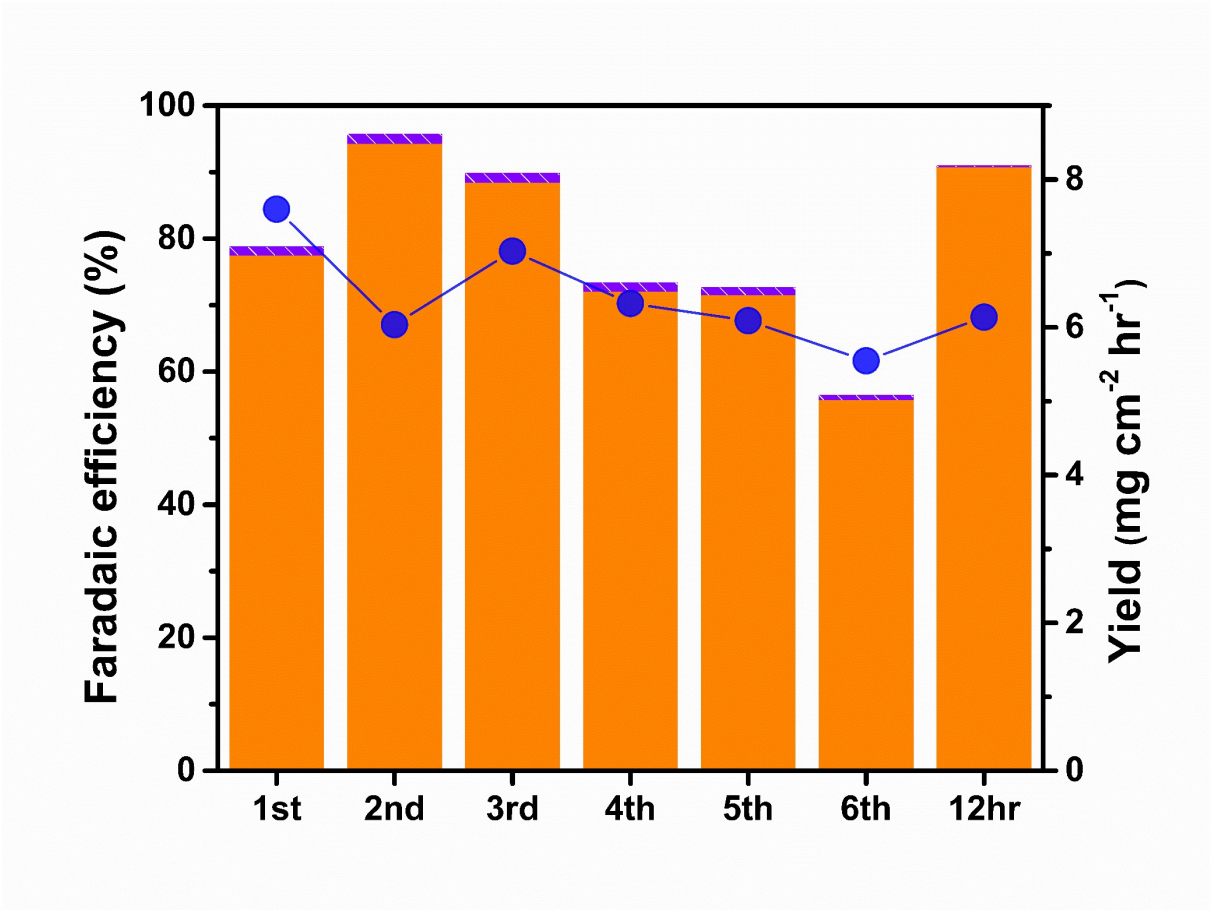

Figure S12. Faradaic efficiency and NH_3 yield during the stability tests (cycling tests & 12 h test).

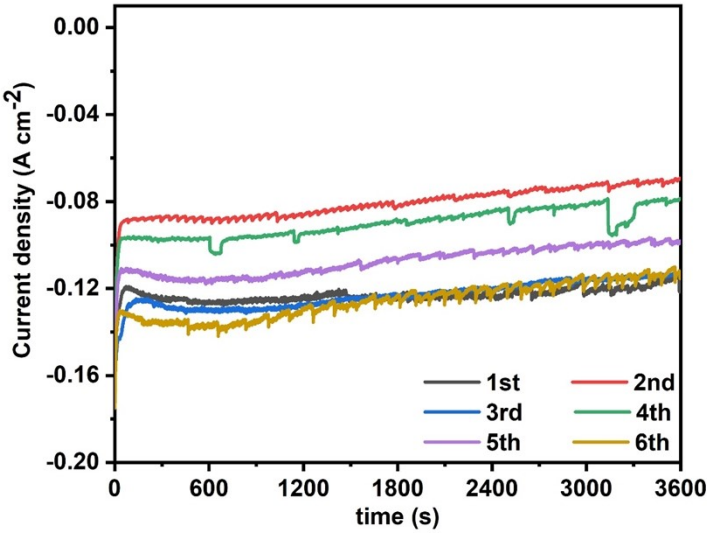

Figure S13. Current densities during the cycling tests.

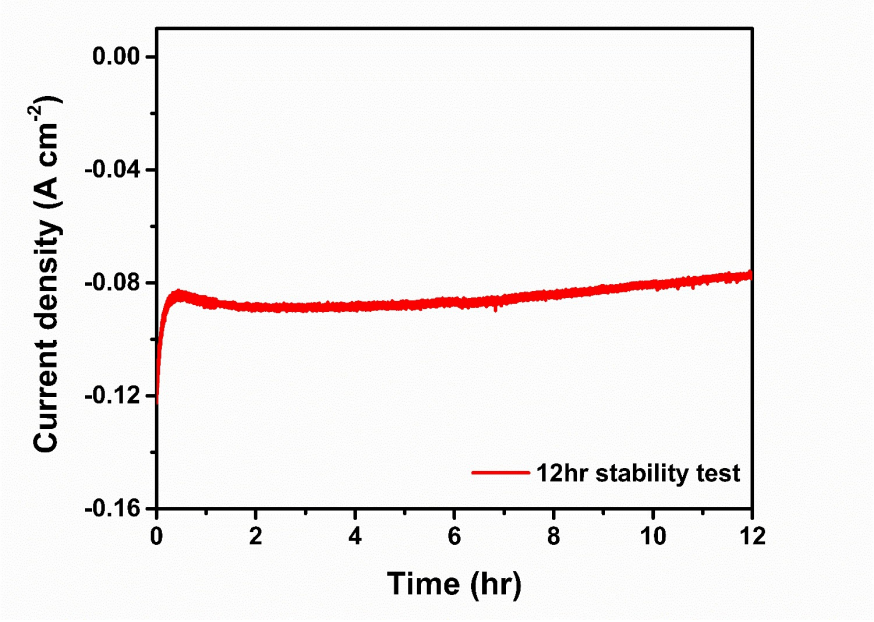

Figure S14. Current density profile measured during the 12 h stability test.

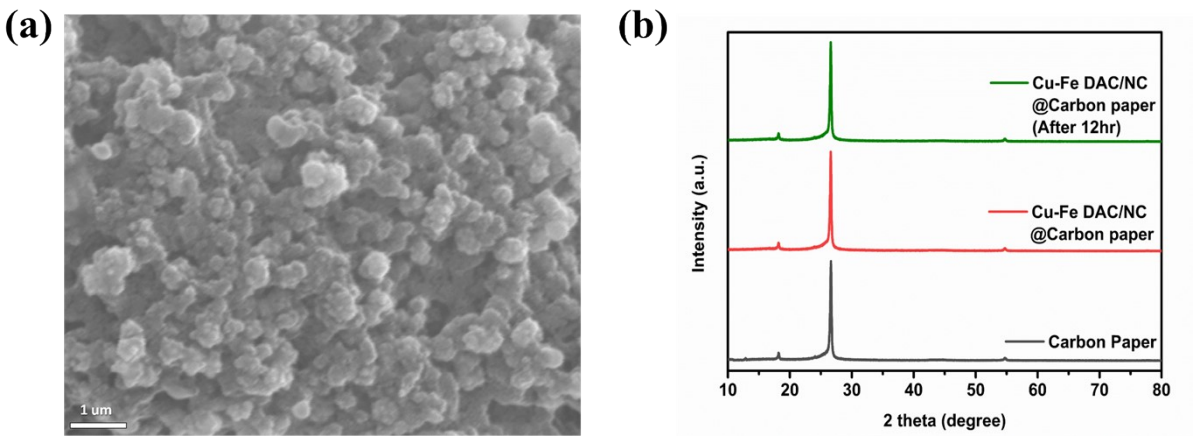

Figure S15. (a) SEM imange of Cu-Fe DAC/NC after the 12 h stability test (b) XRD spectra of Cu-Fe DAC/NC obtained after the 12 h stability test.

Table S1. The ICP-OES results of prepared catalysts.

Samples	Cu (at %)	Fe (at %)
Cu SAC/NC	0.842	-
Fe SAC/NC	-	1.178
Cu-Fe DAC/NC	0.436	0.527

Table S2. The contents of N species of prepared catalysts based on XPS results.

Samples	N (at %)	Graphitic N (%)	Pyridinic N (%)	Oxidized N (%)	Pyrrolic N (%)	M-N (%)
Cu-Fe DAC/NC	3.5	9.3	41.5	5.8	23.3	20.1
Cu SAC/NC	3.8	16.6	33.3	8.3	25.0	16.7
Fe SAC/NC	4.1	9.4	37.7	9.4	28.3	15.1

Table S3. XANES normalization condition of Athena program for prepared catalysts series.

Samples	E0	Pre-edge range	Normalization range	Normalization order
Cu SAC/NC	8987.00	-150 to -30	150 to 745.89	3
Fe SAC/NC	7126.82	-150 to -30	150 to 859.22	3
FeCu DAC/NC	8979.0	-150 to -30	150 to 850	3
FeCu DAC/NC	7125.91	-150 to -30	150 to 400.00	3

Table S4. EXAFS fitting results of Cu and Fe K-edge for the shell of catalysts series.

Samples	Shell	CN[a]	R (Å)[b]	$\triangle E_0$ (eV)[c]	σ (Å^2)[d]	R factor
Cu SAC/NC	Cu-N	3.818	1.942	-5.147	0.0030	1.8703
Fe SAC/NC	Fe-N	3.654	1.949	-7.477	0.0086	1.8703
Cu-Fe DAC/NC	Cu-N	3.917	1.805	-4.162	0.0013	2.0032
Cu-Fe DAC/NC	Fe-N	4.294	1.801	-6.358	0.0030	1.9127

[a] The average coordination number for the coordination shell.
[b] Interatomic distance.
[c] E_0 shift of the path.
[d] Debye-Waller factor.

Table S5. Faradaic efficiencies (%) of products and yield of NH_3 obtained from electrocatalytic NO_3RR on prepared catalysts at different potentials.

Catalyst	E (V vs RHE)	NH_3 FE (%)	NO_2^- FE (%)	H_2 FE (%)	NH_3 yield ($mg \cdot h^{-1} \cdot cm^{-2}$)
Cu SAC/NC	– 0.23	11.3	22.2	25.1	0.78
	– 0.33	21.6	18.3	22.2	1.19
	– 0.43	30.0	15.2	17.1	1.61
	– 0.53	45.3	15.7	13.5	1.98
	– 0.63	30.9	11.2	23.9	2.66
Catalyst	E (V vs RHE)	NH_3 FE (%)	NO_2^- FE (%)	H_2 FE (%)	NH_3 yield ($mg \cdot h^{-1} \cdot cm^{-2}$)
Fe SAC/NC	– 0.23	18.2	23.4	15.1	1.11
	– 0.33	25.1	11.0	13.5	1.43
	– 0.43	47.1	5.9	11.5	2.82
	– 0.53	52.9	1.1	12.5	3.12
	– 0.63	46.5	1.4	20.9	3.59
Catalyst	E (V vs RHE)	NH_3 FE (%)	NO_2^- FE (%)	H_2 FE (%)	NH_3 yield ($mg \cdot h^{-1} \cdot cm^{-2}$)
Cu-Fe DAC/NC	– 0.23	23.3	36.7	15.6	0.72
	– 0.33	35.6	30.5	13.4	1.08
	– 0.43	61.4	18.1	5.5	1.52
	– 0.53	94.3	1.5	0.6	6.04
	– 0.63	57.8	1.2	28.4	5.73

Table S6. Faradaic efficiencies (%) of products and yield of NH_3 obtained from electrocatalytic NO_3RR on Cu-Fe DAC at Cycle test

Catalyst	cycle	NH_3 FE (%)	NO_2^- FE (%)	Total FE (%)	NH_3 yield ($mg \cdot h^{-1} \cdot cm^{-2}$)
Cu-Fe DAC/NC	1	77.9	1.3	79.2	7.60
	2	94.3	1.5	95.8	6.04
	3	88.4	1.5	89.9	7.03
	4	72.1	1.4	73.5	6.32
	5	71.5	1.2	72.7	6.09
	6	55.7	0.8	56.5	5.55
	12hr	90.76	0.23	90.99	6.14

Table S7. The electrochemical nitrate reduction reaction performance comparison with other reported catalyst recently.

Catalysts	NH_3 Faradaic efficiency	NH_3 yield rate	Electrolyte	Reference
Cu-Fe DAC/NC	**94.3%**	**6.04 mg·h^{-1}·cm^{-2}**	**100 mM KNO_3 1 M KOH**	**This work**
Cu-N_1O_2 SACs	96.5 %	3.120 mg h^{-1} cm^{-2}	10 mM KNO_3 0.1 M KOH	[10]
PR-CuNC	94.61 %	3.74 mg h^{-1} cm^{-2}	100 mM KNO_3 0.1 M KOH	[11]
Cu-N_1O_2	96.5 %	3.12 mg h^{-1} cm^{-2}	100 mM KNO_3 0.1 M KOH	[12]
Cu–N–C	84.7 %	4.5 mg h^{-1} cm^{-2}	100 mM KNO_3 0.1 M KOH	[13]
Fe/Cu-HNG	92.51 %	4.41 mg h^{-1} cm^{-2}	100 mM KNO_3 1 M KOH	[14]
Fe−N/P−C	90.3 %	4.50 mg h^{-1} cm^{-2}	100 mM KNO_3 0.1 M KOH	[15]
Fe-MoS_2	98 %	0.51 mg h^{-1} cm^{-2}	0.1 M $NaNO_3$ 0.1 M Na_2SO_4 0.1 M NaOH	[16]
Fe SAC	75%	4 mg h^{-1} cm^{-2}	0.5 M KNO_3 0.1 M K_2SO_4	[17]
Fe SAC	92 %	4.6 mg h^{-1} cm^{-2}	0.5 M KNO_3 0.1 M K_2SO_4	[18]
BCN-Cu	97.37%	3.36 mg h^{-1} cm^{-2}	100 mM KNO_3 0.1 M KOH	[19]
Fe-BCN	97.48%	2.17 mg cm^{-2} h^{-1}	0.5 mM KNO_3 1 M KOH	[20]

Reference

1. P. Giannozzi, O. Baseggio, P. Bonfà, D. Brunato, R. Car, I. Carnimeo, C. Cavazzoni, S. De Gironcoli, P. Delugas, F. Ferrari Ruffino, A. Ferretti, N. Marzari, I. Timrov, A. Urru and S. Baroni, *J. Chem. Phys.*, 2020, 152, 154104. DOI: 10.1063/5.0005082

2. P. E. Blöchl, *Phys. Rev. B*, 1994, 50, 17953. DOI: 10.1103/PhysRevB.50.17953

3. S. Grimme, *J. Comput. Chem.*, 2006, 27, 1787. DOI: 10.1002/jcc.20495

4. J. P. Perdew and Y. Wang, *Phys. Rev. B*, 1992, 45, 13244. DOI: 10.1103/PhysRevB.45.13244

5. S. Grimme, J. Antony, S. Ehrlich and H. Krieg, *J. Chem. Phys.*, 2010, 132, 154104. DOI: 10.1063/1.3382344

6. G. Prandini, A. Marrazzo, I. E. Castelli, N. Mounet, E. Passaro, J. Yu and N. Marzari, *Materials Cloud Archive*, 2021, 76 DOI: 10.24435/materialscloud:2020.0007/v1

7. H. J. Monkhorst and J. D. Pack, *Phys. Rev. B*, 1976, 13, 5188. DOI: 10.1103/PhysRevB.13.5188

8. J. Xu, S. Zhang, H. Liu, S. Liu, Y. Yuan, Y. Meng, M. Wang, C. Shen, Q. Peng, J. Chen, X. Wang, L. Song, K. Li and W. Chen, *Angew. Chem. Int. Ed.*, 2023, 62, e202308044.

9. H. Niu, Z. Zhang, X. Wang, X. Wan, C. Shao and Y. Guo, *Adv. Funct. Mater.*, 2021, 31, 2008533.

10. Y. Liu, Z. Zhuang, Y. Liu, N. Liu, Y. Li, Y. Cheng, J. Yu, R. Yu, D. Wang and H. Li, *Angew. Chem., Int. Ed.*, 2024, 63, e202411396. DOI: 10.1002/anie.202411396

11. Y. Liu, W. Qiu, P. Wang, R. Li, K. Liu, K. M. Omer, Z. Jin and P. Li, *Appl. Catal., B*, 2024, 340, 123228. DOI: 10.1016/j.apcatb.2023.123228

12. Z. Gu, Y. Zhang, Y. Fu, D. Hu, F. Peng, Y. Tang and H. Yang, *Angew. Chem., Int. Ed.*, 2024, 63, e202409125. DOI: 10.1002/anie.202409125

13. J. Yang, H. Qi, A. Li, X. Liu, X. Yang, S. Zhang, Q. Zhao, Q. Jiang, Y. Su, L. Zhang, J. F. Li, Z. Q. Tian, W. L. Wang, A. Wang and T. Zhang, J. *Am. Chem. Soc.*, 2022, 144, 12062. DOI: 10.1021/jacs.2c02262

14. S. Zhang, J. Wu, M. Zheng, X. Jin, Z. Shen, Z. Li, Y. Wang, Q. Wang, X. Wang, H. Wei, J. Zhang, P. Wang, S. Zhang, L. Yu, L. Dong, Q. Zhu, H. Zhang and J. Lu, *Nat. Commun.*, 2023, 14, 3634. DOI: 10.1038/s41467-023-39366-9

15. E. Murphy, B. Sun, M. Rüscher, Y. Liu, W. Zang, S. Guo, Y.-H. Chen, U. Hejral, Y. Huang, A. Ly, I. V. Zenyuk, X. Pan, J. Timoshenko, B. R. Cuenya, E. D. Spoerke, P. Atanassov, *Adv. Mater.*, 2024, 36, 2401133. DOI: 10.1002/adma.202401133

16. L. Wang, P. Guo, Y. Han, C. Han, H. Sun, R. Huang, X. Liu, M. Huang, Z. Mao, X. Yan, A. Du and X. Wang, *Chem. Catal.*, 2024, 4, 100936. DOI: 10.1016/j.checat.2024.100936

17. Z. Y. Wu, M. Karamad, X. Yong, Q. Z. Huang, D. A. Cullen, P. Zhu, C. A. Xia, Q. F. Xiao, M. Shakouri, F. Y. Chen, J. Y. Kim, Y. Xia, K. Heck, Y. F. Hu, M. S. Wong, Q. L. Li, I. Gates, S. Siahrostami and H. T. Wang, *Nat. Commun.*, 2021, 12, 2870. DOI: 10.1038/s41467-021-23115-x
18. H. Chen, C. Zhang, L. Sheng, M. Wang, W. Fu, S. Gao, Z. Zhang, S. Chen, R. Si, L. Wang and B. Yang, J. *Hazard. Mater.*, 2022, 434, 128892. DOI: 10.1016/j.jhazmat.2022.128892
19. Y. Liu, J. Wei, Z. Yang, L. Zheng, J. Zhao, Z. Song, Y. Zhou, J. Cheng, J. Meng, Z. Geng and J. Zeng, *Nat. Commun.*, 2024, 15, 3619. DOI: 10.1038/s41467-024-48035-4
20. X. Lu, J. Wei, H. Lin, Y. Li and Y. Li, *ACS Appl. Nano Mater.*, 2024, 7, 14654. DOI: 10.1021/acsanm.4c02221